JBC ARTICLE

The cytoplasmic tail of rhodopsin triggers rapid rod degeneration in kinesin-2 mutants

Received for publication, March 1, 2017, and in revised form, August 24, 2017 Published, Papers in Press, August 30, 2017, DOI 10.1074/jbc.M117.784017

Dong Feng[‡], Zhe Chen[‡], Kuang Yang[‡], Shanshan Miao[‡], Bolin Xu[‡], Yunsi Kang[‡], Haibo Xie[‡], and Chengtian Zhao[‡§¶1]

From the [‡]Institute of Evolution and Marine Biodiversity, Ocean University of China, Qingdao 266003, China, the [§]Laboratory for Marine Biology and Biotechnology, Qingdao National Laboratory for Marine Science and Technology, Qingdao 266003, China, and the [¶]Ministry of Education Key Laboratory of Marine Genetics and Breeding, College of Marine Life Sciences, Ocean University of China, Qingdao 266003, China

Edited by F. Anne Stephenson

Photoreceptor degeneration can lead to blindness and represents the most common form of neural degenerative disease worldwide. Although many genes involved in photoreceptor degeneration have been identified, the underlying mechanisms remain to be elucidated. Here we examined photoreceptor development in zebrafish *kif3a* and *kif3b* mutants, which affect two subunits of the kinesin-2 complex. In both mutants, rods degenerated quickly, whereas cones underwent a slow degeneration process. Notably, the photoreceptor defects were considerably more severe in *kif3a* mutants than in *kif3b* mutants. In the cone photoreceptors of *kif3a* mutants, opsin proteins accumulated in the apical region and formed abnormal membrane structures. In contrast, rhodopsins were enriched in the rod cell body membrane and represented the primary reason for rapid rod degeneration in these mutants. Moreover, removal of the cytoplasmic tail of rhodopsin to reduce its function, but not decreasing rhodopsin expression levels, prevented rod degeneration in both *kif3a* and *kif3b* mutants. Of note, overexpression of full-length rhodopsin or its cytoplasmic tail domain, but not of rhodopsin lacking the cytoplasmic tail, exacerbated rod degeneration in *kif3a* mutants, implying an important role of the cytoplasmic tail in rod degeneration. Finally, we showed that the cytoplasmic tail of rhodopsin might trigger rod degeneration through activating the downstream calcium signaling pathway, as drug treatment with inhibitors of intracellular calcium release prevented rod degeneration in *kif3a* mutants. Our results demonstrate a previously unknown function of the rhodopsin cytoplasmic domain during opsin-triggered photoreceptor degeneration and may open up new avenues for managing this disease.

Photoreceptor cells consist of highly polarized neurons with a distinct photosensitive compartment, termed the outer segment (OS).[2] The OS comprises a modified cilium with a large stack of disk membranes containing opsins, the most abundant protein of the cell. The retina contains two types of classic photoreceptors, rods and cones, which are responsible for vision at low and high levels, respectively. Because of a lack of protein translation machinery, all of the OS protein components must be first synthesized in the inner segment (IS) and transported to the OS through a narrow channel called the connecting cilium (1).

Similar to cilia in other cells, the connecting cilium contains the microtubule-based axoneme with a "9 + 0" configuration. The initiation and maintenance of connecting cilia require an elaborate intraflagellar transport (IFT) process that is driven by two classic motors, kinesin-2 (anterograde) and cytoplasmic dynein 2 (retrograde). The heterotrimeric kinesin-2 motor is composed of three subunits, including two kinesin-2 motor subunits (KIF3A and KIF3B) and one nonmotor subunit (KAP3) (2, 3). *In vitro* studies suggest that KIF3C, another kinesin-2 protein, may substitute for KIF3B in the kinesin-2 motor (4, 5). In addition, KIF17, another member of the kinesin-2 family, functions as a dimer during ciliary transport (3).

Kinesin-2 family members mediate protein transport in photoreceptor cells. Loss of function of KIF3A in the mouse retina interrupts the transport machinery and leads to rapid photoreceptor cell death (6–8). In zebrafish, mutation in *kif3a* gene leads to mispositioning of the basal bodies and photoreceptor cell death (9). Dysfunction of Kif3b, however, affects only a subset of cilia, and photoreceptor connecting cilium is initially absent but then partially recovered latterly (10). Although inhibition of Kif17 by dominant-negative expression or morpholino-based knockdown may affect OS development, zebrafish *kif17* mutants are able to grow to adulthood with normal photoreceptor functions (10–12). Furthermore, another study has suggested that KIF17 is dispensable for photoreceptor development (13).

Photoreceptor degeneration occurs in many human genetic disorders, including retinitis pigmentosa (RP), the most common form of inherited retinal degeneration (14). Previous studies suggest that ectopic opsin accumulation leads to photoreceptor cell death and that diminishing expression of the *rho* gene can delay the degeneration of rod photoreceptors (7, 15). However, the requirement of kinesin-2 for opsin transportation

This work was supported by National Natural Science Foundation of China Grants 31372274, 31422051, and 81301718; Shandong Provincial Natural Science Foundation Grant JQ201506; and Fundamental Research Funds for the Central Universities Grant 201562029. The authors declare that they have no conflicts of interest with the contents of this article.
This article contains supplemental Figs. S1–S8 and Table S1.

[1] To whom correspondence should be addressed. Tel.: 86-532-8203-2962. E-mail: chengtian_zhao@ouc.edu.cn.

[2] The abbreviations used are: OS, outer segment; IS, inner segment; IFT, intraflagellar transport; RP, retinitis pigmentosa; dpf, days post-fertilization; hpf, hours post-fertilization; qPCR, quantitative PCR; WISH, whole-mount *in situ* hybridization; PFA, paraformaldehyde.

remains controversial. Mutation of either the *IFT* or *KIF3A* gene results in rod degeneration together with mislocalization of rhodopsin, indicating that IFT mediates opsin transport (6, 16, 17). Further analysis using the fluorescence recovery after photobleaching method in live cells also shows that KIF3A plays a role during opsin transport (18). Conversely, recent studies suggest that opsin transport may still occur without the function of both KIF3 and KIF17 motors (13, 19, 20).

The structure and function of photoreceptor cells are similar in zebrafish and humans. The zebrafish retina contains five types of photoreceptor cells, including one rod photoreceptor cell type and four cone photoreceptor cell types. According to their absorption spectra and morphology, cone photoreceptors are classified as short single cones sensitive to ultraviolet light, long single cones sensitive to blue light, and double cones comprised of a red-sensitive and a green-sensitive cell (21, 22). Cone and rod photoreceptors form a highly ordered mosaic in the adult retina (23). Previously, we reported that rod photoreceptors degenerated in zebrafish *kif3b* mutants, although the underlying mechanisms are yet to be understood (10). Here we further generated zebrafish *kif3a* mutants and investigated rod and cone development therein. As for *kif3b* mutants, rod photoreceptors in *kif3a* mutants exhibited a faster degeneration process than cones. Further experiments demonstrated that opsins were accumulated in the apical part of cone photoreceptors, whereas most rod opsins localized to the cell membrane. We next generated a zebrafish mutant allele lacking the carboxyl-terminal cytoplasmic tail of rhodopsin and found that rods were maintained in *kif3a/rho* double mutants. Furthermore, we showed that the cytoplasmic domain plays a key role during rod degeneration, as overexpression of full-length opsin or the cytoplasmic domain alone, but not the form lacking the cytoplasmic domain, accelerated rod degeneration in *kif3a* mutants. Finally, drug treatment with calcium channel blockers increased the rod survival ratio in *kif3a* mutants, suggesting that the calcium signaling pathway is involved in photoreceptor degeneration.

Results

Rapid rod degeneration in kif3a mutants

To elucidate the mechanisms underlying the degeneration of rod photoreceptors observed following *kif3b* dysfunction in early zebrafish embryos (10), in this study, we further generated *kif3a* mutants using CRISPR/Cas9 methods (supplemental Fig. S1, *A–C*). Similar to other ciliary mutants, zebrafish *kif3a* mutants displayed body curvature at 3 days post fertilization (dpf). Whole-mount immunostaining with an anti-acetylated α-tubulin antibody demonstrated that all cilia were absent in *kif3a* mutant larvae (supplemental Fig. S1, *D–I*), which differs from the consequences of mutation of the other two kinesin-2 genes, *kif3b* and *kif17* (9–11). The complete absence of cilia has also been described in another *kif3a* mutant line derived from *N*-ethyl-*N*-nitrosourea mutagenesis (data not shown and Ref. 9). These results indicate that Kif3a is indispensable for ciliogenesis in zebrafish.

We next examined photoreceptor development in *kif3a* mutants by crossing these animals to *Tg(Xla.Rho:GFP)*, a rod-specific transgenic line driven by the *Xenopus rhodopsin* promoter (referred to here as *XOPS-GFP*) (23). At 3 dpf, the GFP signals in the retina of wild-type and *kif3a* mutants were indistinguishable (supplemental Fig. S2). However, *kif3a* mutants displayed a rapid decrease of GFP signals in the retina in the following 48 h of development, and only scattered GFP signals could be observed in the sections of mutant retina at 5 dpf (Fig. 1, *A–C*, and supplemental Fig. S2). We further analyzed the expression of rod-specific genes via quantitative PCR (qPCR) and whole-mount *in situ* hybridization (WISH) and found that these genes were all down-regulated in *kif3a* mutants at 5 dpf (Fig. 1, *D–F*). These results suggest that mutation of *kif3a* leads to fast rod degeneration from 3 to 5 dpf, which is similar to that observed in *kif3b* mutants (Fig. 1, *D* and *F*) (10).

Cone photoreceptor development in kif3a mutants

In *kif3b* mutants, cone photoreceptors survive longer than 5 dpf, as shown by both WISH and qPCR analysis (Fig. 2, *A* and *B*). Similarly, WISH results for two cone opsin genes, *uv* and *green*, demonstrated similar staining levels at 5 dpf in the retinae of *kif3a* and wild-type larvae (Fig. 2*A*), whereas qPCR analysis indicated that the expression of cone-specific genes decreased slightly (Fig. 2*C*). Next, we examined cone development via whole-mount immunostaining using the zpr-1 antibody, which recognizes Arr3a and selectively labels cell body of the red- and green-sensitive double cones (22, 24). In contrast to the fast degeneration of rods, the majority of double cones were still present at 4 dpf in the retinae of *kif3a* mutants, and only a small number of cones degenerated at 5 dpf, suggesting that cones degenerate much slower than rods in *kif3a* mutants (Fig. 2*D* and supplemental Fig. S2). Similarly, the double cones of *kif3b* mutants showed a grossly normal staining pattern comparable with that of wild-type siblings at 5 dpf. In contrast, the cone photoreceptors in another ciliary mutant, *ovl*, which harbors a mutation that affects one of the IFT proteins, Ift88, displayed a much more severe degeneration phenotype at the same developmental stage (Fig. 2*D* and supplemental Fig. S2).

Next, we crossed *kif3a* mutants to a stable transgenic line, *Tg(hsp:GFP-CT44)*, which expresses GFP fused to the 44 C-terminal amino acids of rhodopsin driven by a heat shock promoter (25, 26). In wild-type embryos, this fusion protein could be easily transported to the outer segment within 4 h after heat shock (25). We reasoned that such GFP signals might localize to the inner cell membrane of photoreceptors because of the dysfunction of IFT in *kif3a* mutants. However, we noticed that the majority of GFP signals accumulated at the apical region of photoreceptor cells in *kif3a* mutants after heat induction at 5 dpf (Fig. 2*E*). Further immunostaining results with Tom20, a mitochondrial marker, suggested that these GFP fusion proteins localized apically to the mitochondria (Fig. 2*E*). Similarly, such protein accumulation also occurs in UV light-sensitive photoreceptor cells, as shown using another stable transgenic line expressing tdTomato fused to the same outer segment targeting signals driven by the *sws1* promoter (27, 28). Noticeably, a small amount of fusion proteins also localized to the cell membrane and synapse in the mutants (Fig. 2*E*, *arrows*). These results suggest that opsin proteins may be sequestered apically in the mutant photoreceptors. Interestingly, most of these

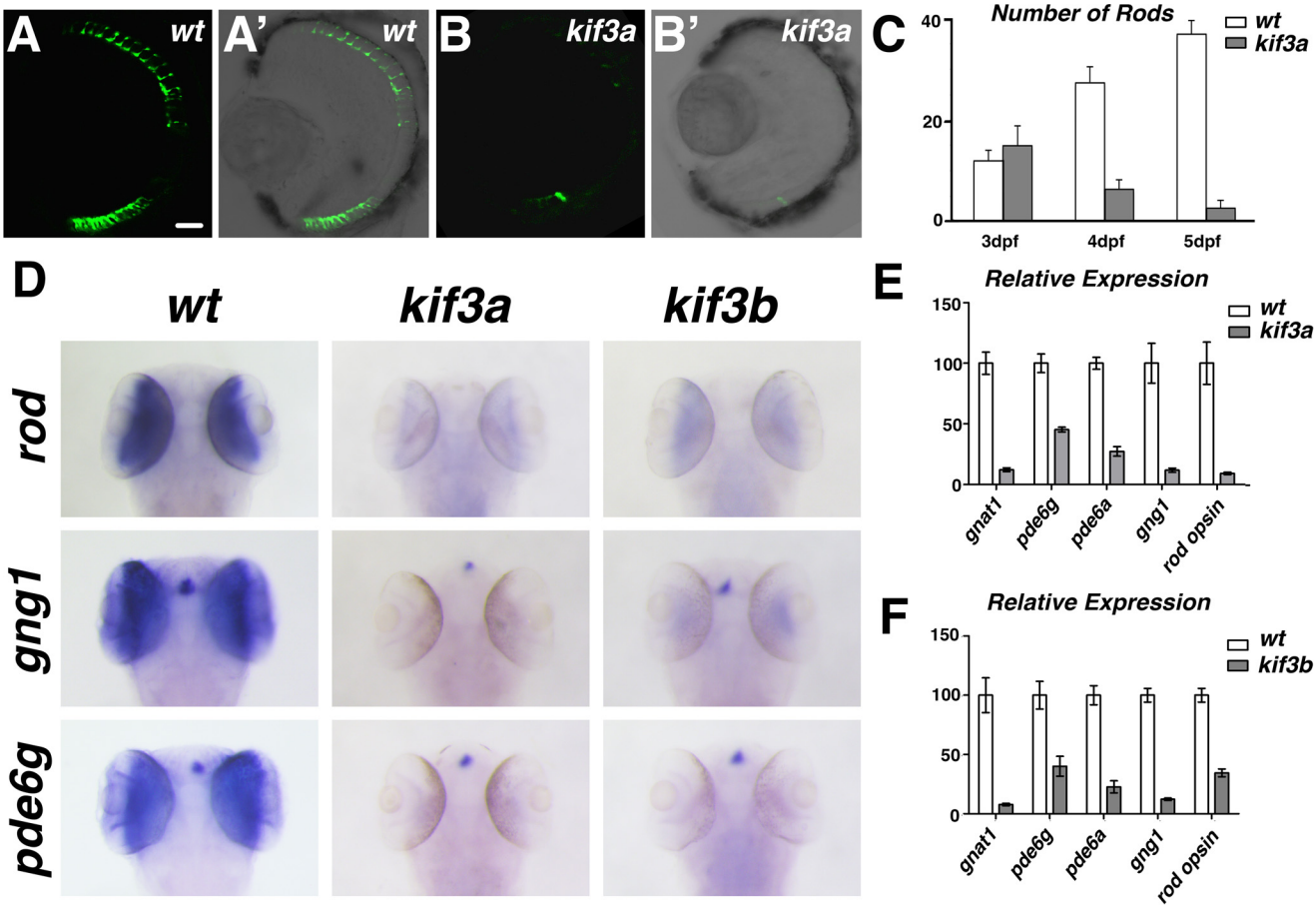

Figure 1. Rod degeneration in kinesin-2 mutants. *A–B′*, transverse sections through the central retina of 5-dpf-old wild-type (*A* and *A′*) or *kif3a* mutant larva (*B* and *B′*) harboring a GFP transgene driven by the *Xenopus* rhodopsin promoter. *C*, the number of rods in the retinae of wild-type or *kif3a* mutant larvae at different stages as indicated. *D*, whole-mount *in situ* hybridization of wild-type, *kif3a*, and *kif3b* larvae at 5 dpf with rod-specific genes as indicated. *E*, qPCR results showing the expression of rod-specific genes at 5 dpf in *kif3a* mutant and control sibling embryos. *F*, qPCR results showing the expression of rod-specific genes at 5 dpf in *kif3b* mutant and control sibling embryos. *Scale bar* = 25 μm.

ectopic opsins did not colocalize with Rom1b, another outer segment membrane protein (supplemental Fig. S3). Next, we performed electron microscopy analysis of the retina of 5-dpf larvae. As shown in Fig. 2, *F–I*, irregular membrane structures were consistently formed on the exteriors of mitochondria in the photoreceptors of *kif3a* mutants. Considering that rods already degenerate at this stage, these results suggest that the majority of opsins localized to the apical region of cone photoreceptors in *kif3a* mutants.

Redundancy between Kif3b and Kif3c

In contrast to the complete absence of cilia in *kif3a* mutants, loss of function of Kif3b only results in ciliogenesis defects in a subset of cilia (Fig. 3*F*) (10). Robust cilia were still present in the central nervous system (CNS) of *kif3b* mutant embryos on a *Tg(bactin2:Arl13b-GFP)* transgenic strain background (data not shown). Similarly, although rods degenerated quickly in *kif3b* mutants, the cones were relatively normal compared with those of *kif3a* mutants (Fig. 2, *A–D*, and supplemental Fig. S2). The mild phenotype of *kif3b* mutants may be related to the presence of the Kif3c protein, which can also bind to Kif3a *in vitro* (4). Zebrafish carry two *KIF3C* homologues, *kif3ca* and *kif3cb*, both of which are mainly expressed in the CNS, although *kif3ca* is expressed at a relatively higher level (Fig. 3, *A–D*). To test *in vivo* functional redundancy between Kif3c and Kif3b, we further generated zebrafish *kif3ca* mutants (Fig. 3*E*). Although cilia developed normally in *kif3ca* mutants, *kif3b/kif3ca* double mutants failed to develop cilia in ear cristae and photoreceptor cells, suggesting that Kif3ca is involved in the formation of these cilia in *kif3b* mutants (Fig. 3*F*). In addition, the photoreceptor layer was also severely disorganized in the double mutants (Fig. 3*F*). Next, we generated a stable transgenic line expressing GFP fused to the N terminus of the Kif3ca protein and driven by a heat shock promoter (Fig. 3*G*). We found that all examined cilia that were absent in *kif3b* mutants could be fully rescued upon heat induction, including motile, non-motile, single, and multiple cilia (Fig. 3, *H–P*). These results demonstrate that Kif3b and Kif3ca are interchangeable during ciliary transport.

Next, we focused on photoreceptor development in *kif3b* mutants. The expression of rod-specific genes was maintained following Kif3ca protein overexpression (Fig. 4, *A* and *I*). Rod outer segments and photoreceptor-connecting cilia were recovered as well (Fig. 4, *B–H*). In contrast, overexpression of another member of the kinesin-2 protein family, Kif17, could not prevent rod degeneration, although the cilia could be rescued in several other tissues, including the spinal cord (Fig. 4*A*) (10). Finally, overexpression of neither *kif3ca* nor *kif3cb* can

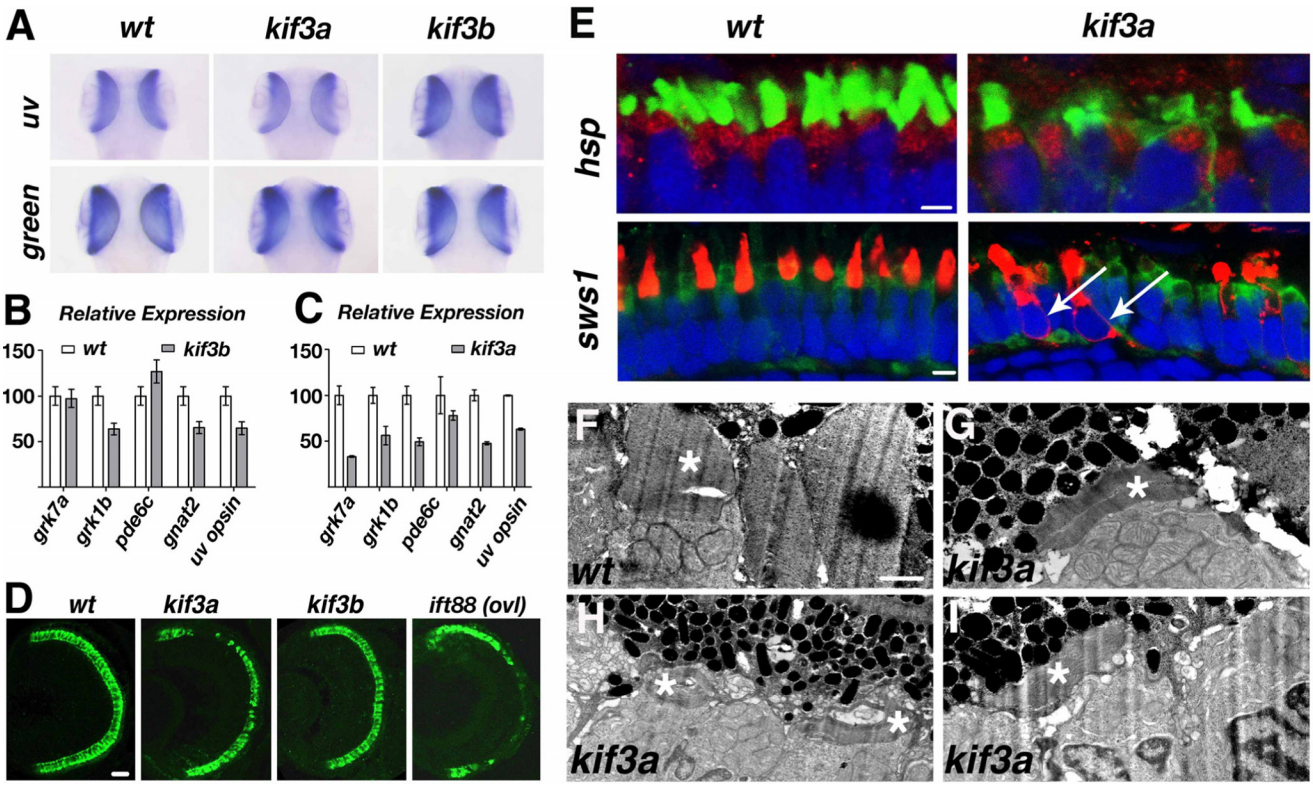

Figure 2. Cone development in kinesin-2 mutants. *A*, whole-mount *in situ* hybridization of two cone opsin genes in the retinae of 5 dpf wild type and *kif3a* and *kif3b* mutants. *B*, qPCR results of cone-specific genes at 5 dpf in *kif3b* and sibling embryos. *C*, qPCR results of cone-specific genes at 5 dpf in *kif3a* and sibling embryos. *D*, confocal images showing the cell body of double cone photoreceptors visualized by zpr-1 antibody in 5-dpf wild-type and mutant embryos as indicated. *E*, confocal images of transverse sections through the central retinae of wild-type and mutant embryos as indicated. *Top panels*, the *green* channel shows the localization of GFP-CT44 driven by a heat shock promoter. Mitochondria were visualized with an anti-Tom20 antibody (*red*). *Bottom panels*, the *red* channel shows the localization of tdTomato-CT44 driven by the *sws1* promoter. The cell bodies of double cones were labeled with zpr-1 antibody in the *green* channel. In both images, nuclei were stained with DAPI. *F*, transmission electron microscopy (TEM) of photoreceptor outer segments in the wild-type retina of a 5-dpf larva (*asterisks*). *G–I*, electron micrographs showing abnormal membrane structures in the retinae of 5-dpf *kif3a* mutants (*asterisks*). *Scale bars* = 25 μm in *D*, 2.5 μm in *E*, and 1 μm in *F–I*.

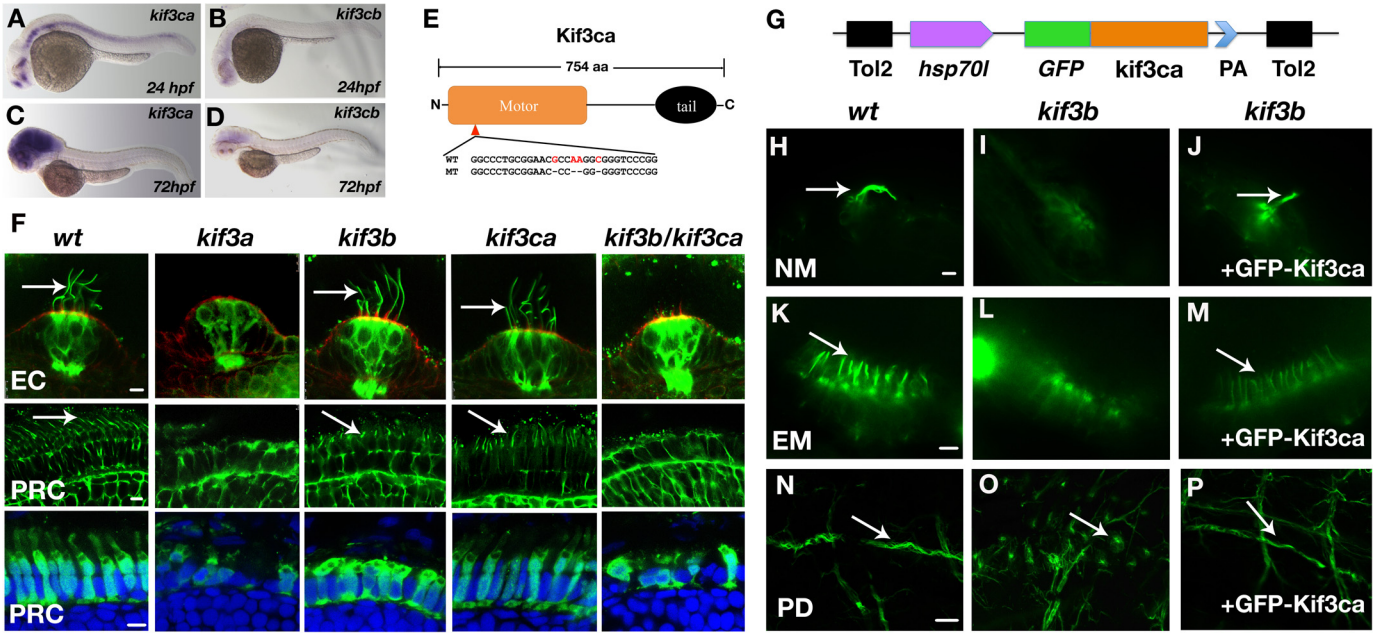

Figure 3. Redundancy between Kif3b and Kif3ca during ciliogenesis. *A–D*, whole-mount *in situ* hybridization results of the *kif3ca* and *kif3cb* genes in 24-hpf and 72-hpf embryos as indicated. *E*, protein structure and sequences of wild-type and *kif3ca* mutant alleles. *F*, confocal images showing cilia in ear cristae (*EC*, *top panels*) and photoreceptor cells (*PRC*, *center panels*) in 5-dpf wild-type and mutant embryos as indicated. *Bottom panels*, cell body shapes of double cone photoreceptors visualized by zpr-1 antibody in 5-dpf wild-type and mutant larvae as indicated. *G*, diagram of the constructs used to generate the *GFP-kif3ca* transgene. *H–P*, confocal images showing cilia in different organs as indicated. *Arrows* indicate cilia labeled with anti-acetylated α-tubulin antibody (*green*). In *F*, F-actin was counterstained by phalloidin in *red* (*top panels*), and nuclei were labeled with DAPI (*bottom panels*). *NM*, neuromast; *EM*, ear macula; *PD*, pronephric duct. *Scale bars* = 5 μm.

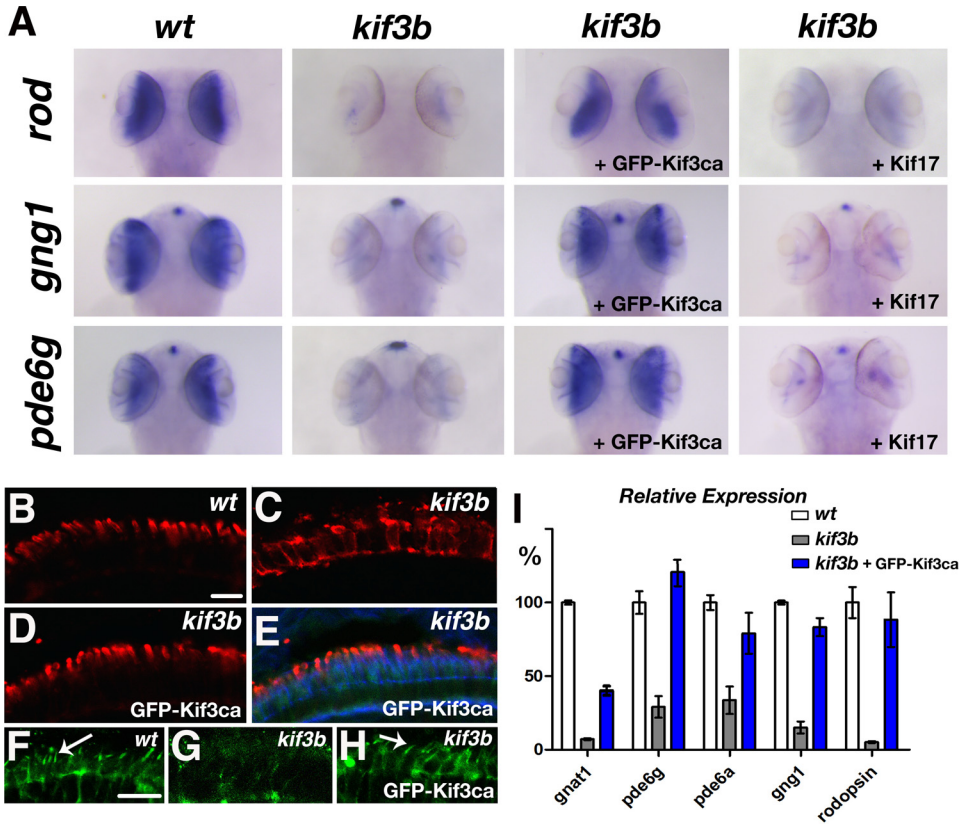

Figure 4. Redundancy between Kif3b and Kif3c during photoreceptor development. *A*, whole-mount *in situ* hybridization with rod-specific genes in 5-dpf wild-type and mutant larvae as indicated. *B–E*, confocal images from the central retinae of 5-dpf larvae showing rod outer segments labeled with zpr-3 antibody. In *E*, the *green* channel shows expression of the GFP-Kif3ca transgene, and F-actin was counterstained by phalloidin (*blue*). *F–H*, confocal images showing photoreceptor connecting cilia, visualized with anti-acetylated tubulin antibody in 5-dpf wild-type and mutant larvae as indicated. *Arrows* indicate photoreceptor-connecting cilia. *I*, qPCR results of rod-specific genes in 5-dpf wild-type and mutant larvae as indicated. *Scale bars* = 10 μm.

rescue cilia or photoreceptor defects in *kif3a* mutants, although both can rescue ciliary defects in *kif3b* mutants, suggesting the essential function of Kif3a during ciliogenesis (supplemental Figs. S4 and S5). Together, these results suggest that function of Kif3ca and Kif3b are redundant in ciliogenesis, which is the reason underlying the mild phenotype in *kif3b* mutants.

Excess opsin accumulation contributes to the rapid degeneration of rod photoreceptors

Considering that opsin mislocalization is one of the causes of photoreceptor cell death, we further investigated opsin distribution using the *Tg(hsp:GFP-CT44)* transgenic line. Specifically, the transgene was heat-induced at 3.5 dpf when most of the rods were still present in the *kif3a* mutants. In the photoreceptors of wild-type embryos, the GFP signals exclusively accumulated in the outer segments 12 h after heat shock, whereas robust signals were still present in the cell membrane of the photoreceptors in *kif3a* mutants (data not shown). To better distinguish cones and rods, we isolated single photoreceptors and simultaneously labeled them with zpr-1 and zpr-3 antibodies. Zpr-3 is a monoclonal antibody that can recognize outer segments of both rods and short double cones (29, 30). In the isolated mutant photoreceptors, the short double cones would be labeled with both antibodies (cell membrane, zpr-3; cell body, zpr-1), whereas only the cell membrane would be labeled in rod cells (Fig. 5*A*). Comparison of the average fluorescence intensity in the cell membrane between double cones and rods identified that the GFP signals were significantly higher in the membrane of rods than those of cones (Fig. 5, *A* and *B*). We further investigated the distribution of endogenous proteins by staining with an anti-bovine rhodopsin antibody, 4D2. Because the 4D2 antibody recognizes both rod and double cone opsins in zebrafish (supplemental Fig. S6), we performed this analysis using the *XOPS-GFP* transgenic line to identify rod photoreceptors. Similarly, rod cell membrane was found to contain a higher level of opsins than those of cones (Fig. 5, *E* and *F*).

Next, we repeated the opsin transport experiments in *ift88* mutants, which exhibit rapid degeneration of both rods and cones (supplemental Fig. S2). As shown in Fig. 5*C*, both rod and cone cell membranes contained robust but similar fluorescence intensities, indicating that opsin transport was similarly affected in cones and rods lacking Ift88 proteins (Fig. 5, *C* and *D*). The high GFP intensity in the cell membrane was consistent with the rapid photoreceptor degeneration in *kif3a* and *ift88* mutants. These results suggest that excess opsin accumulation in the cell membrane of rods contributes to their fast degeneration in *kif3a* mutants.

Disruption of rhodopsin function prevents rod degeneration in kif3 mutants

As the rod cell membrane contains a higher level of opsin proteins, we reasoned that elimination of rhodopsin might prevent rod degeneration in *kif3* (*kif3a* and *kif3b*) mutants. To test this hypothesis, we generated a mutant line harboring a 5-bp

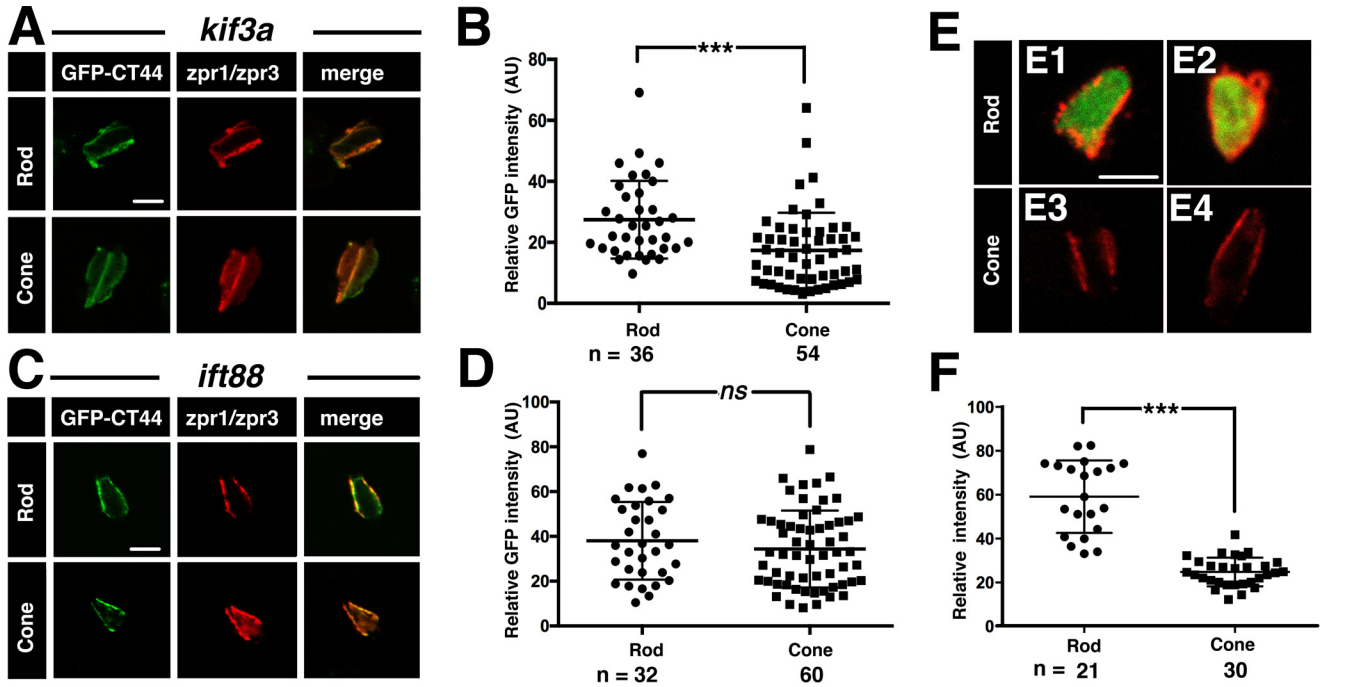

Figure 5. Ectopic opsin accumulation in *kif3a* and *ift88* mutants. *A* and *C*, confocal images showing GFP-CT44 signals in the cell membrane of individual photoreceptor cells in *kif3a* (*A*) and *ift88* (*C*) mutants. The photoreceptor cells were labeled with both zpr-1 and zpr-3 antibodies (*red*). Note that only the green-sensitive cone was labeled in the double cones (*A*). *B* and *D*, scatterplot showing the average GFP intensity in the cell membrane of rods and double cones as indicated. The number of individual photoreceptor cells is shown at the *bottom*. *E*, confocal images showing the localization of opsin proteins in the cell membrane of rods and cones stained with anti-rhodopsin 4D2 antibody (*red*). The *green* channel indicates the expression of GFP in rods driven by the *XOPS* promoter. *F*, quantification of the average fluorescence intensity of endogenous opsins in rods and double cones as indicated. The number of individual photoreceptor cells counted is shown at the *bottom*. ***, $p < 0.001$; *ns*, not significant. *Scale bars* = 5 μm.

deletion in the *rho* gene, which encodes a truncated protein lacking the entire cytoplasmic carboxyl terminus (amino acids 315–354) (Fig. 6*A*). Whole-mount immunostaining and ultrastructural results suggested that the photoreceptor cell layer appeared to be grossly normal in the mutants at the larval stage (Fig. 6, *B–E*, and data not shown). Notably, the truncated proteins still localized to the outer segments at the larval stage, as shown by zpr-3 and 4D2 antibody staining (Fig. 6, *D* and *E*, and data not shown). In contrast, the majority of rod outer segments were missing in the adult retina (Fig. 6, *F–I*). The rod nuclear layer was also significantly thinner than that of wild-type siblings (Fig. 6, *F–I*). In the remaining rod photoreceptors, the mutant rhodopsins ectopically localized to the cell membrane (Fig. 6*I*, *arrows*). These results suggest that the rod cells had degenerated during development in this mutant line.

We further generated *kif3a/rho* and *kif3b/rho* double mutants and investigated the development of rod photoreceptors at 5 dpf. WISH and qPCR results with rod-specific genes showed that the expression level was largely maintained in the double mutants (Fig. 7, *A–D* and *H*, and supplemental Fig. S7). Although outer segments did not form, the photoreceptor cell layers were grossly intact in the double mutants (Fig. 7, *E–G*). Notably, rod degeneration was also prevented in *kif3a/rho*$^{+/-}$ mutants (Fig. 7*H*). Strikingly, the expression level of the mutant *rho* gene remained unchanged, and the truncated proteins were still enriched in the cell membrane in the double mutants (Fig. 7, *D*, *G*, and *H*). These results suggest that the cytoplasmic tail plays a role during rod degeneration.

The rhodopsin cytoplasmic tail mediates photoreceptor degeneration in kif3 mutants

To further test the role of the rhodopsin cytoplasmic tail during photoreceptor degeneration, we overexpressed wild-type or mutant rhodopsin in *kif3a* mutants and investigated rod development therein. In wild-type embryos, overexpression of either full-length or mutant rhodopsin lacking the cytoplasmic tail did not affect rod development (Fig. 7, *I* and *Q*). In contrast, overexpression of full-length rhodopsin accelerated rod degeneration in *kif3a* mutants, as suggested by the number of GFP-positive rod photoreceptors (Fig. 7, *J*, *L*, and *Q*). The number of rod cells appeared to be indistinguishable between mutant retinae injected with the cytoplasmic tail– deficient rhodopsin and uninjected mutant controls (Fig. 7, *J*, *K*, and *Q*). Strikingly, overexpression of the cytoplasmic tail alone by heat shock induction significantly affected the survival of rod photoreceptors (Fig. 7, *M–P* and *R*). These results strongly suggest that the rhodopsin cytoplasmic tail participates in photoreceptor degeneration in *kif3a* mutants.

In the outer segments, rhodopsin activates its G-protein, transducin, and initiates the phototransduction signaling pathway. We speculated that rhodopsin might activate the apoptosis signaling pathway via its cytoplasmic tail when localized to the cell body membrane ectopically. As calcium is a key element in apoptotic signaling, we tested the effects of modulating calcium signaling on rod development in *kif3* mutants. First, we treated the *kif3a* mutants and siblings with thapsigargin, which helps raise intracellular free calcium by inhibiting the endoplas-

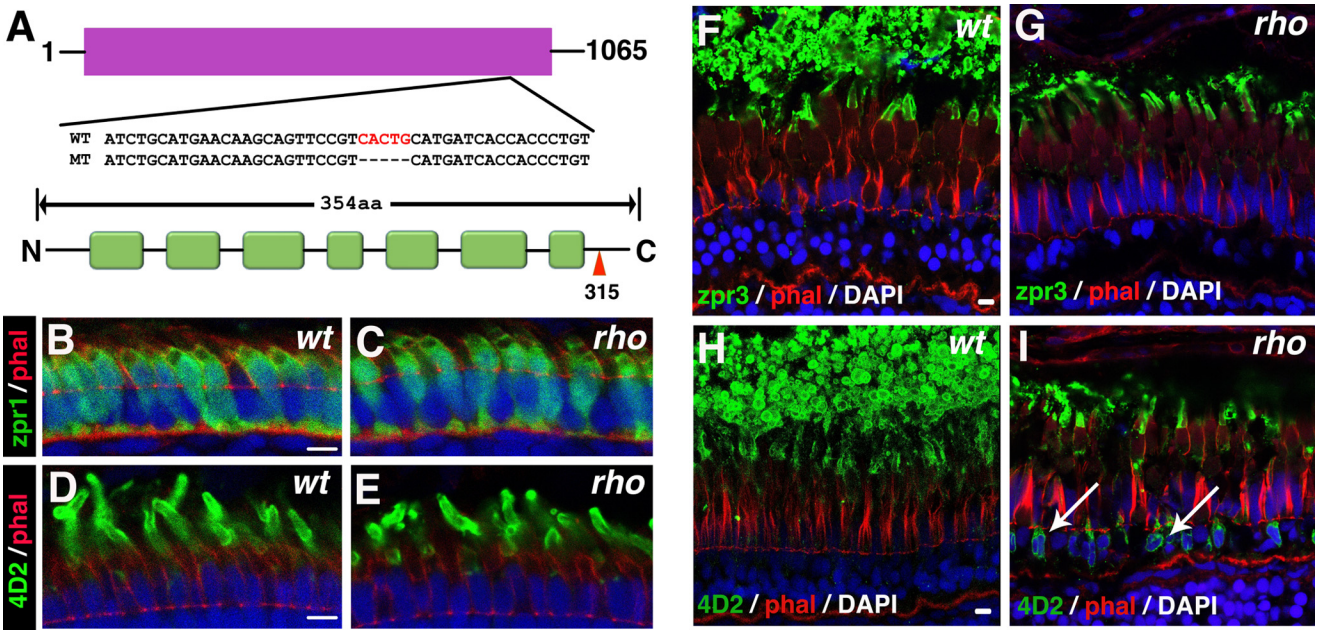

Figure 6. Phenotype of *rho* mutants. *A*, diagram showing the genomic structure of the zebrafish *rho* gene and the sequences of mutant and wild-type alleles. The seven transmembrane domains of rhodopsin are shown at the *bottom*. The *red arrowhead* marks the truncated site in the mutant allele. *aa*, amino acids. *B–E*, confocal images of transverse sections through the central retinae of 5-dpf wild-type and mutant larvae visualized by zpr-1 antibody (*B* and *C*) to label cell bodies of double cone photoreceptors or 4D2 antibody (*D* and *E*) to label rod outer segments. *F–I*, confocal images of transverse sections through the central retinae of mutant and wild-type adult fish stained with zpr-3 antibody (*F* and *G*) and 4D2 antibody (*H* and *I*). In *B–I*, the *red* channel shows staining of phalloidin to indicate the layer of the retina. The nuclei were labeled with DAPI. The *arrows* in *I* indicate ectopic opsin proteins in the plasma membrane. *Scale bars* = 5 μm.

mic reticulum Ca-ATPase (31). As shown in Fig. 8, thapsigargin treatment exaggerated rod degeneration in both *kif3a* and *kif3b* mutants (Fig. 8, *A–E*). In contrast, drug treatment with two intracellular calcium release inhibitors, dantrolene or 2-aminoethoxydiphenyl borate, increased the number of surviving rod cells significantly (Fig. 8, *F* and *G*). These results suggest that ectopic rhodopsin may trigger a calcium-dependent apoptosis pathway via its cytoplasmic tail.

Discussion

Members of the kinesin-2 family play diverse roles during vertebrate ciliogenesis. In zebrafish, mutation in *kif3b* gene results in defects in a subset of cilia, whereas almost all cilium formation is affected in *kif3a* mutants (Refs. 9, 10 and this study). In contrast, Kif3c and Kif17 appear to be dispensable for zebrafish development (9, 10). During photoreceptor development, kinesin-2 proteins drive the movement of IFT complexes and facilitate the transport of cargo proteins through the connecting cilium. Our results show that both Kif3a and Kif3b are required for photoreceptor development. Although not necessary, Kif3ca could substitute for Kif3b to maintain protein transport in the photoreceptors as well as in the other types of cilia examined. Notably, dysfunction of either Kif3a or Kif3b led to rapid degeneration in rod photoreceptors, whereas cones survived longer than rods in the mutants. In *kif3b* mutants, cones degenerated slower than in *kif3a* mutants, possibly because of the presence of small amounts of Kif3ca in *kif3b* mutants that maintain the IFT mechanisms.

The apical accumulation of opsin proteins in cone photoreceptors represents a notable phenomenon in *kif3a* mutants. We consider that such accumulation occurs mainly in cone photoreceptors, as robust opsin fusion proteins were still present on the apical regions when the larvae were heat induced as late as 7 dpf, at which time the majority of rods had degenerated (data not shown). Our results demonstrated that rods and cones differed from each other upon removal of the *kif3a* gene. In photoreceptor cells of zebrafish larva, the outer segments start to form at around 2.5 dpf, concomitant with the initial synthesis of opsin and other outer segment proteins in the inner segments. These outer segment proteins are first transported to the base of the connecting cilium, driven by cytoplasmic dynein 1 motors (Fig. 8*H*), and then transported to their destination through the connecting cilium. Subsequently, the outer segments start to expand with the delivery of additional opsins, membrane proteins, and other scaffold proteins. In *kif3a* mutants, these proteins can still be transported to the basal body region; however, no connecting cilium is formed because of the lack of IFT, which is necessary for tubulin delivery, a key component of the ciliary axoneme (32, 33). In rod photoreceptors, membrane proteins, including rhodopsin, are transported to the base of the outer segments to form a new membrane disk. However, consequent to the lack of a connecting cilium, these proteins will be initially concentrated at the cell membrane in the apical region and then quickly dispersed to the entire plasma membrane by diffusion (Fig. 8*H*). Such ectopic rhodopsin proteins may trigger the apoptosis signaling pathway via their cytoplasmic tails, which would further activate calcium signaling and lead to eventual photoreceptor degeneration. In *kif3/rho* double mutants, lack of the cytoplasmic tail prevents the activation of cell apoptosis signaling, and rod degeneration is blocked (Fig. 8*H*). In contrast, cones appear to have different transport mechanisms because of the continuity of the membrane disks, which can quickly deliver opsins to the entire outer

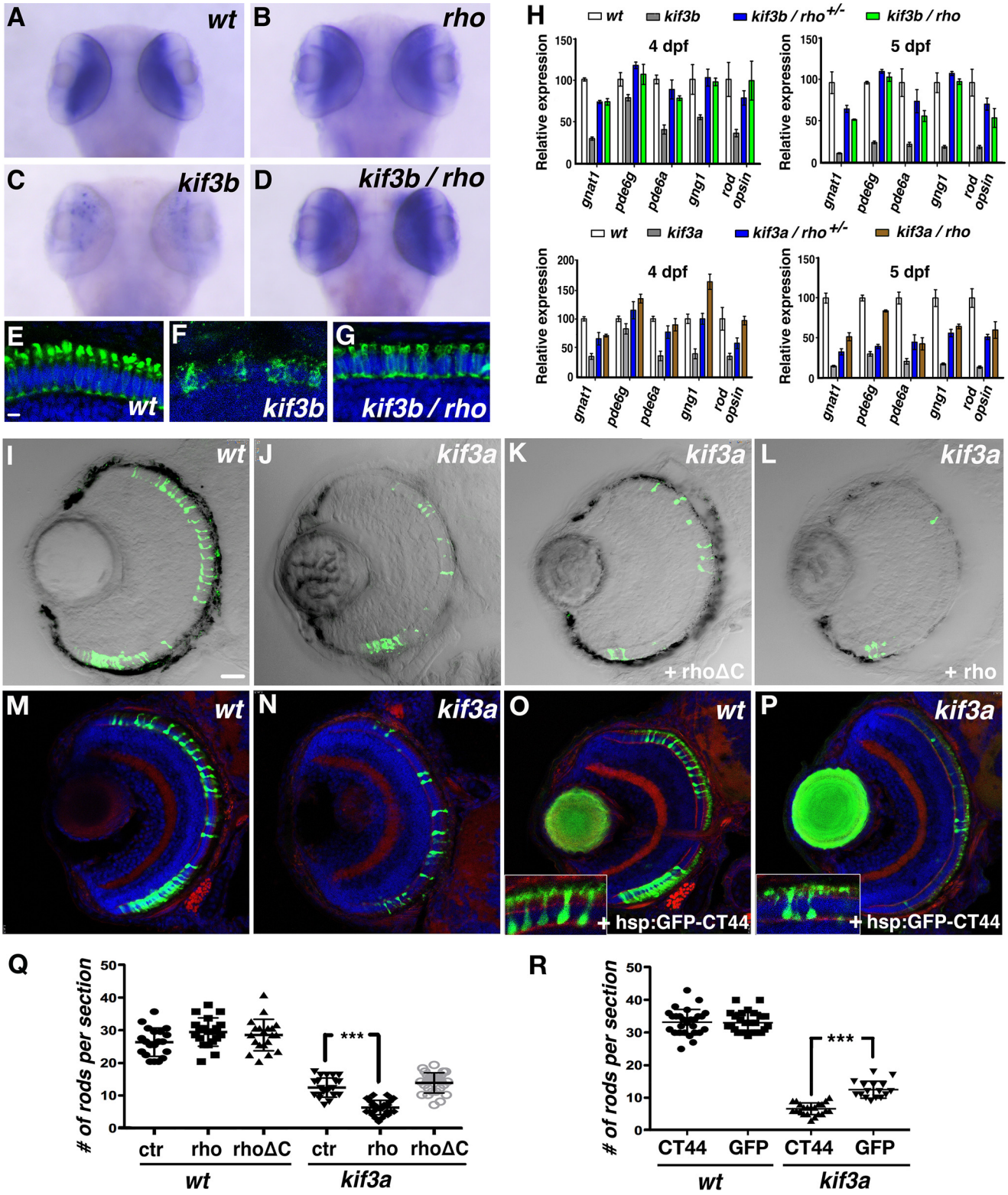

Figure 7. The cytoplasmic tail of rhodopsin mediates rod degeneration in *kif3a* and *kif3b* mutants. *A–D*, whole-mount *in situ* hybridization with the *rho* gene in 5-dpf wild-type and mutant larvae as indicated. *E–G*, confocal images of transverse sections showing the localization of opsin proteins labeled by 4D2 antibody in wild-type and mutant larvae as indicated. The nuclei were counterstained by DAPI. *H*, qPCR results with rod-specific genes in wild-type and mutant larvae at different stages as indicated. *I–L*, confocal images of transverse frozen sections through the central retinae of 4-dpf wild-type and mutant *XOPS-GFP* transgenic larvae injected with full-length or the truncated form of *rho* as indicated. *Green* channels indicate GFP expression in rod photoreceptors. *M–P*, representative confocal images showing the expression of GFP in rod photoreceptors in the retinae of 4-dpf wild-type and mutant transgenic larvae without (*M* and *N*) or with (*O* and *P*) overexpression of the cytoplasmic tail of rhodopsin. The enlargement shows the details of GFP expression in the *XOPS-GFP*/Tg (*hsp:GFP-CT44*) double transgenic line. Note that the GFP-CT44 fusion protein localizes to the apical region of photoreceptors. *Q*, statistical results showing the number of rod photoreceptors per section through the central retina as indicated in *I*. *R*, quantification of the number of rod photoreceptors per section in wild-type and mutant retinae as indicated. ***, $p < 0.001$. *Scale bars* = 5 μm in *E–G* and 25 μm in *I–P*.

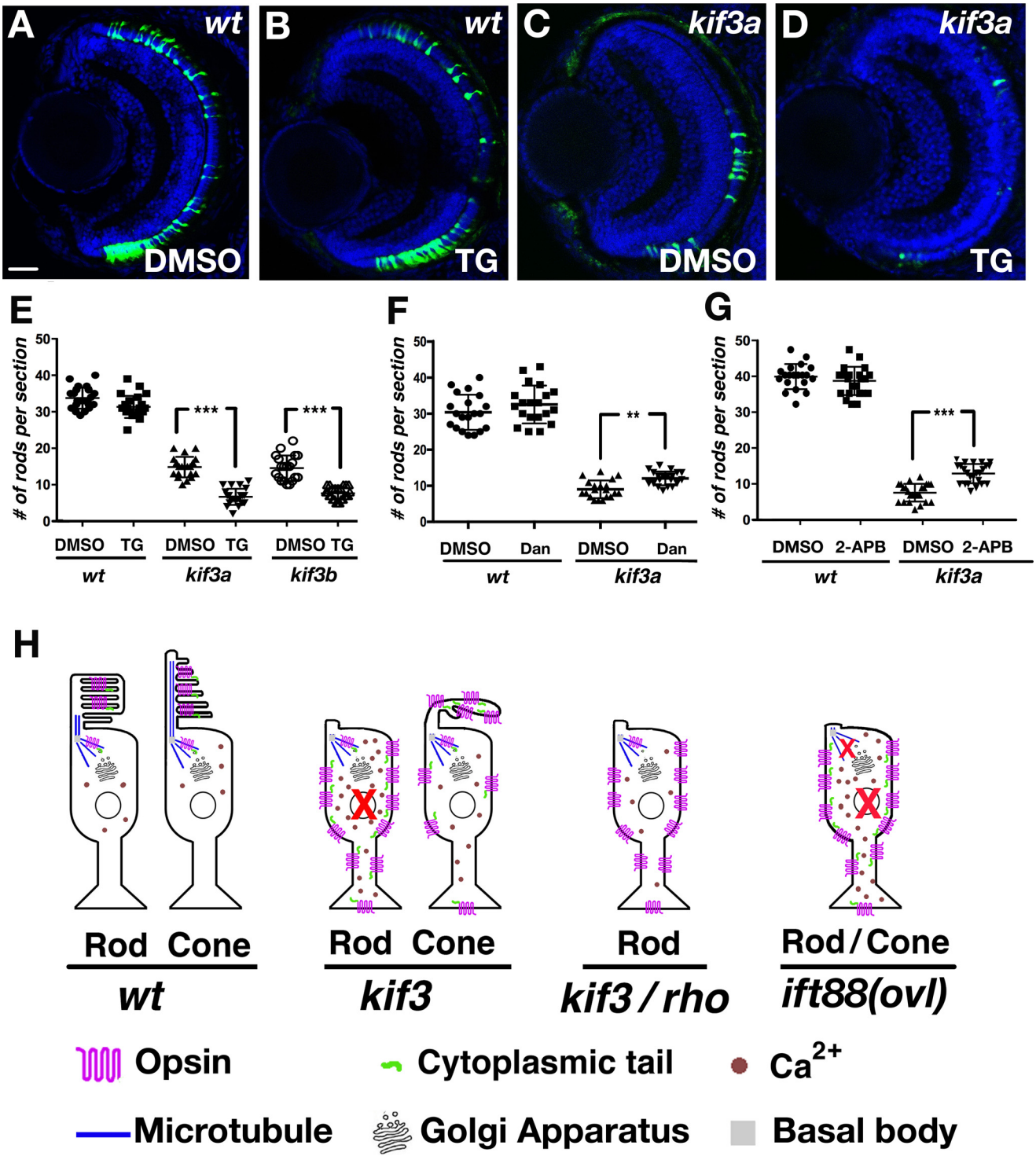

Figure 8. Elevation of cytoplasmic calcium results in photoreceptor degeneration in *kif3* mutants. *A–D*, representative confocal images showing the expression of GFP in rod photoreceptors in the retinae of 4-dpf wild-type (*A* and *B*) and mutant transgenic larvae (*C* and *D*) treated with DMSO or thapsigargin (*TG*) as indicated. *E*, quantification of the number of rod photoreceptors per section in 4-dpf wild-type and mutant retinae treated with DMSO or thapsigargin as indicated. *F*, quantification of the number of rod photoreceptors per section in DMSO- or dantrolene (*Dan*)-treated 5-dpf embryos. *G*, quantification of the number of rod photoreceptors per section in DMSO- or 2-aminoethoxydiphenyl borate–treated 5-dpf embryos. *H*, summary of photoreceptor degeneration in *kif3* and *ift88* mutants. In wild-type photoreceptors, opsins were synthesized in the inner segment and transported to the outer segment in both rods and cones. In *kif3* mutants, ectopic opsins accumulate in the cell membrane of rods and activate the calcium signaling pathway, leading to rapid rod degeneration. In contrast, abnormal membrane structures develop in the apical region of cone photoreceptors, which leads to a lower concentration of opsin protein in the cell membrane and a longer survival time. In *kif3/rho* double mutants, opsin proteins are still enriched in the cell membrane, but lack of a cytoplasmic tail prevents activation of the downstream cell apoptosis pathway. In *ift88(ovl)* mutants, both rods and cones contain higher amounts of ectopic opsins in the cell membrane and degenerate quickly (See "Discussion" for more details). **, $p < 0.01$; ***, $p < 0.001$. *Scale bar* = 25 μm.

segments over a short time period (34, 35). Although the connecting cilium fails to form in the cones of *kif3a* mutants, opsins can still be transported, and abnormal membrane structures start to form because of the lack of the ciliary axoneme. Under these conditions, a substantial portion of cone opsins become sequestered in the apical region, and only small quantities of opsins are diffused to the plasma membrane, which improves the survival ratio of cone photoreceptors (Fig. 8*H*).

In comparison, both cones and rods degenerate rapidly in *ift88(ovl)* mutants, indicating the different roles of Ift88 and Kif3 motors in opsin transport. IFT88 has been reported previously to localize in both the ciliary axoneme and the periciliary cytoplasm in photoreceptor cells and may participate in the transport of post-Golgi vesicles to the ciliary membrane during early development stages (36, 37). When Ift88 is absent, the first step of opsin transport will be interrupted, and these membrane proteins will consequently be misdirected to the cytoplasmic membrane, resulting in rod and cone degeneration (Fig. 8*H*).

Opsin mislocalization constitutes one of the major causes of photoreceptor cell degeneration (7, 15). We further confirmed this by showing that interference with the function of rhodopsin could inhibit the degeneration of rod photoreceptors in *kif3* mutants. Notably, the rhodopsin present in the *rho* mutants lacked only the last cytoplasmic domain, and its expression level was similar to that of control siblings. Because the truncated proteins could be transported to the outer segments, it is possible that mutant rhodopsin will activate phototransduction, as it contains all three cytoplasmic loops that are necessary for the binding of G-protein (38). Of note, the cytoplasmic tail plays an essential role during deactivation of rhodopsin and, hence, the termination of the visual signals in that it contains several phosphorylation sites that are necessary for the binding of G-protein–coupled receptor kinase and arrestin (39–41). Thus, the absence of the cytoplasmic tail may lead to excessive signaling because of overactive rhodopsin, constituting the main reason of progressive photoreceptor degeneration in humans (42, 43) and zebrafish mutants.

The recovery of rod degeneration in *kif3/rho* double mutants suggested that the carboxyl-terminal cytoplasmic domain participated in the cell death process. In wild-type embryos, overexpression of either full-length or truncated proteins did not affect rod development, suggesting that ectopic localization of rhodopsin in the cell body membrane is a prerequisite for inducing rod degeneration. Similarly, thapsigargin treatment did not lead to significant rod degeneration in Tg(*hsp*:GFP-CT44) transgenic embryos, where the overexpressed CT44 mainly localizes to the outer segments (supplemental Fig. S8). Conversely, the means by which the cytoplasmic tail triggers cell apoptosis remains unknown. The signaling transduction pathways in the cell body differ considerably from those of the outer segment. It is possible that this ectopic G-protein–coupled receptor binds to certain cytoplasmic G-proteins and activates downstream signaling pathways, as suggested by previous study in *Ambystoma tigrinum* (44). One of the phenotypes associated with such signaling pathways is the increase of internal Ca^{2+} signals, as suggested by the drug treatment results. Further experiments are necessary to decipher the mechanisms underlying this apoptotic pathway.

Finally, the mutation site in *rho* zebrafish mutants (H315) is close to the human Q312ter rhodopsin mutation, which might also result in complete loss of the entire cytoplasmic tail (45). Interestingly, human patients harboring the Q312ter mutation displayed mild retinal disease compared with other rhodopsin mutations (45), possibly suggesting that the cytoplasmic tail may also function during rods degeneration in human RP patients. In conclusion, we found a novel function of the cytoplasmic tail during ectopic rhodopsin-triggered rod degeneration. Future studies of this signaling pathway may benefit the treatment of human RP.

Experimental procedures

Zebrafish strains

All zebrafish strains were maintained at a 14-h light/10-h dark cycle at 28 °C. CRISPR/Cas9 technology was used to generate zebrafish *kif3a, kif3ca*, and *rho* mutants. The following target sites for single guide RNA (sgRNA) were used: 5′-GAGGAGGTGAGAGATCTGTT-3′, 5′-GGCCCTGCGGAACGCCAAGG-3′, and 5′-TCACTGCATGATCACCACCC-3′. *Cas9* mRNA, single guide RNA synthesis, and mutant screening were similar to those described previously (46).

Whole-mount in situ hybridization and immunohistochemistry

For *in situ* hybridization, rod- and cone-specific genes were either purchased from Open Biosystems as reported previously (10) or cloned from a wild-type cDNA library into pGEM-T vectors. Probe preparation and hybridization were carried out using standard protocols (47). For immunohistochemistry, the following antibodies were used: anti-acetylated α-tubulin (1:500, Sigma), zpr-3 (1:500, Zebrafish International Resource Center), zpr-1 (1:500, Zebrafish International Resource Center), Tom20 (1:200, Abcam), and anti-rhodopsin 4D2 (1:500, Abcam). For larva fish, cryosectioning and antibody staining were performed as described previously (48). To isolate single adult photoreceptors, eyeballs were dissected from euthanatized adult fish and washed in L15 medium. After removal of the cornea and lens, the retina was put into 100 μl of L15 medium and briefly rinsed several times. The supernatant, which contains single rod photoreceptors, was transferred to poly-L-lysine–coated slides, incubated for 1.5 h at 28 °C, and then fixed in 4% paraformaldehyde (PFA) overnight at 4 °C. The leftovers, which contained cone photoreceptors and other neurons, were also fixed in 4% PFA. The following immunostaining steps were the same as for larva photoreceptors. After staining, the confocal images were collected on a Leica TCS Sp8 upright confocal microscope.

Quantitative PCR

The primers used for qPCR are summarized in supplemental Table S1. The PCR reaction was set up using Eva-Green Master Mix (ABM) and performed on an ABI 7500 real-time PCR system (Applied Biosystems). The amplification condition parameters were 95 °C for 15 s, followed by 40 cycles of 95 °C for 5 s, 60 °C for 15 s, and 72 °C for 35 s, and each sample had triplicate reactions. Relative gene expression levels were quantified using

the comparative Ct method ($2^{-\Delta\Delta Ct}$ method) based on Ct values for target genes and zebrafish *β-actin*.

Opsin accumulation analysis

To better control the expression level of the GFP-CT44 fusion protein, we first generated a stable transgenic line expressing *GFP-CT44* driven by a heat shock promoter and then crossed to the *kif3a*$^{+/-}$ or *ift88*$^{+/-}$ heterozygotic fish. The mutant larvae containing the transgene were heat-induced at 42 °C for 1 h at 3.5 dpf and then collected at 4 dpf. After euthanasia with Tricaine, the eyeballs were collected and digested with papain (30 units/ml, Roche) in L15 medium at 37 °C for 5 min and then fixed in 4% PFA overnight at 4 °C. After fixation, the samples were ground, seeded onto a poly-lysine–coated slide, and dried at 37 °C. Immunohistochemistry was performed using zpr-1 and zpr-3 antibodies simultaneously as described previously (48). For endogenous experiments, the *kif3a*$^{+/-}$ heterozygotic fish was crossed to the *XOPS-GFP* transgene, and anti-bovine rhodopsin 4D2 antibody was used to label endogenous opsin protein. For quantitation of opsin accumulation, the fluorescence intensity was calculated by drawing a line through each side of the cell membrane using ImageJ software (National Institutes of Health). The average fluorescence intensity per cell was used to evaluate opsin accumulation.

Electron microscopy

Wild-type and *kif3a* mutant larvae were fixed overnight in 2.5% glutaraldehyde in 0.1 M PBS. The samples were washed three times in PBS and fixed again in 1% osmium tetroxide. After that, embryos were washed, gradually dehydrated to 100% acetone, and then embedded in Epon812 resin. Ultrathin sections were collected and stained with uranyl acetate and lead citrate. The sections were observed on a transmission electron microscope (JEM-1200EX) and imaged with Olympus Soft Imaging Solutions.

Overexpression and pharmaceutical treatments

For rescue experiments, the full-length *kif3ca* gene was fused to the C terminus of *GFP* and cloned into the Tol2 Gateway vector driven by a heat shock promoter. The stable transgenic line was identified and crossed to *kif3b* heterozygotic mutants for phenotypic analysis. For mRNA overexpression, full-length *kif3cb* or *kif17* genes were PCR-amplified and cloned into the PXT7 vector. The mRNA was synthesized using the Ambion T7 transcription kit and injected into zebrafish embryos at a concentration of 300 ng/μl. For *rho* overexpression experiments, full-length or mutant (△C) *rho* genes were PCR-amplified and cloned into the PXT7 vector with the following primers: forward, 5′-CGGAATTCACCATGAACGGTACAGAGGGACC-3′; reverse (full-length), 5′-CCGCTCGAGTTACGCCGGAGACACGGAGC-3′; reverse (△C), 5′-CCGCTCGAGTCAACGGAACTGCTTGTTCATGC-3′. The synthesized mRNA was injected into zebrafish embryos carrying the *XOPS-GFP* transgene at the one-cell stage with a concentration of 200 ng/μl. The injected embryos containing the *XOPS-GFP* transgene were collected at 4 dpf and cryosectioned with a Leica CM1850 cryostat. Sections from the center of the retina were captured for evaluation of rod development. For overexpression of the cytoplasmic tail of rhodopsin, we generated zebrafish *kif3a* mutants carrying *Tg(hsp:GFP-CT44)* and *XOPS-GFP* double transgenes. Both the mutant larvae and their siblings were heat-induced at 42 °C for 2 h at 3.5 dpf, transferred to 28 °C, and collected at 4 dpf for rod degeneration analysis.

For drug treatment, transgenic embryos were treated either with dantrolene (50 μM, Sigma) or 2-aminoethoxydiphenyl borate (0.2 μM, Sigma) from 3 dpf to 5 dpf and then fixed in 4% PFA for rod degeneration analysis. For thapsigargin treatment, transgenic embryos were incubated at 1 μM for 10 h at 3.5 dpf and then fixed in 4% PFA for evaluation of rod degeneration. For *XOPS-GFP*/Tg (*hsp:GFP-CT44*) double-transgenic embryos, the larvae were first heat-induced at 42 °C for 2 h at 3.5 dpf and then treated with 1 μM thapsigargin for 10 h either immediately after heat induction or at 4.5 dpf. After that, the treated embryos were fixed in 4% PFA for evaluation of rod degeneration.

Statistical analysis

Scatterplot data are presented as mean ± S.D. as indicated in the figure legends. Statistical significance was evaluated using a *t* test, and $p < 0.05$ was taken to be statistically significant.

Author contributions—C. Z. designed all experiments. D. F. performed most of the experiments, including immunohistochemistry, q-PCR, *in situ* hybridization, and electron microscopic analysis. Z. C., Y. K., and H. X. performed the mutant and transgenic analyses. K. Y., B. X., and S. M. performed the mutant screen for kif3a and rho fish. D. F. and C. Z. analyzed the data and wrote the manuscript.

Acknowledgments—We thank Bo Dong and Hongyan Li for helpful comments on an earlier version of this manuscript. We also thank Shoji Kawamura and Jarema Malicki for constructs and fish strains.

References

1. Kennedy, B., and Malicki, J. (2009) What drives cell morphogenesis: a look inside the vertebrate photoreceptor. *Dev. Dyn.* **238,** 2115–2138
2. Song, Z., Zhang, X., Jia, S., Yelick, P. C., and Zhao, C. (2016) Zebrafish as a model for human ciliopathies. *J. Genet. Genomics* **43,** 107–120
3. Scholey, J. M. (2013) Kinesin-2: a family of heterotrimeric and homodimeric motors with diverse intracellular transport functions. *Annu. Rev. Cell Dev. Biol.* **29,** 443–469
4. Muresan, V., Abramson, T., Lyass, A., Winter, D., Porro, E., Hong, F., Chamberlin, N. L., and Schnapp, B. J. (1998) KIF3C and KIF3A form a novel neuronal heteromeric kinesin that associates with membrane vesicles. *Mol. Biol. Cell* **9,** 637–652
5. Yang, Z., and Goldstein, L. S. (1998) Characterization of the KIF3C neural kinesin-like motor from mouse. *Mol. Biol. Cell* **9,** 249–261
6. Marszalek, J. R., Liu, X., Roberts, E. A., Chui, D., Marth, J. D., Williams, D. S., and Goldstein, L. S. (2000) Genetic evidence for selective transport of opsin and arrestin by kinesin-II in mammalian photoreceptors. *Cell* **102,** 175–187
7. Lopes, V. S., Jimeno, D., Khanobdee, K., Song, X., Chen, B., Nusinowitz, S., and Williams, D. S. (2010) Dysfunction of heterotrimeric kinesin-2 in rod photoreceptor cells and the role of opsin mislocalization in rapid cell death. *Mol. Biol. Cell* **21,** 4076–4088
8. Jimeno, D., Feiner, L., Lillo, C., Teofilo, K., Goldstein, L. S., Pierce, E. A., and Williams, D. S. (2006) Analysis of kinesin-2 function in photoreceptor cells using synchronous Cre-loxP knockout of Kif3a with RHO-Cre. *Invest. Ophthalmol. Vis. Sci.* **47,** 5039–5046

9. Pooranachandran, N., and Malicki, J. J. (2016) Unexpected roles for ciliary kinesins and intraflagellar transport proteins. *Genetics* **203,** 771–785
10. Zhao, C., Omori, Y., Brodowska, K., Kovach, P., and Malicki, J. (2012) Kinesin-2 family in vertebrate ciliogenesis. *Proc. Natl. Acad. Sci. U.S.A.* **109,** 2388–2393
11. Insinna, C., Pathak, N., Perkins, B., Drummond, I., and Besharse, J. C. (2008) The homodimeric kinesin, Kif17, is essential for vertebrate photoreceptor sensory outer segment development. *Dev. Biol.* **316,** 160–170
12. Insinna, C., Humby, M., Sedmak, T., Wolfrum, U., and Besharse, J. C. (2009) Different roles for KIF17 and kinesin II in photoreceptor development and maintenance. *Dev. Dyn.* **238,** 2211–2222
13. Jiang, L., Tam, B. M., Ying, G., Wu, S., Hauswirth, W. W., Frederick, J. M., Moritz, O. L., and Baehr, W. (2015) Kinesin family 17 (osmotic avoidance abnormal-3) is dispensable for photoreceptor morphology and function. *FASEB J.* **29,** 4866–4880
14. Ferrari, S., Di Iorio, E., Barbaro, V., Ponzin, D., Sorrentino, F. S., and Parmeggiani, F. (2011) Retinitis pigmentosa: genes and disease mechanisms. *Curr. Genomics* **12,** 238–249
15. Tsujikawa, M., and Malicki, J. (2004) Intraflagellar transport genes are essential for differentiation and survival of vertebrate sensory neurons. *Neuron* **42,** 703–716
16. Pazour, G. J., Baker, S. A., Deane, J. A., Cole, D. G., Dickert, B. L., Rosenbaum, J. L., Witman, G. B., and Besharse, J. C. (2002) The intraflagellar transport protein, IFT88, is essential for vertebrate photoreceptor assembly and maintenance. *J. Cell Biol.* **157,** 103–113
17. Krock, B. L., and Perkins, B. D. (2008) The intraflagellar transport protein IFT57 is required for cilia maintenance and regulates IFT-particle-kinesin-II dissociation in vertebrate photoreceptors. *J. Cell Sci.* **121,** 1907–1915
18. Trivedi, D., Colin, E., Louie, C. M., and Williams, D. S. (2012) Live-cell imaging evidence for the ciliary transport of rod photoreceptor opsin by heterotrimeric kinesin-2. *J. Neurosci.* **32,** 10587–10593
19. Jiang, L., Wei, Y., Ronquillo, C. C., Marc, R. E., Yoder, B. K., Frederick, J. M., and Baehr, W. (2015) Heterotrimeric kinesin-2 (KIF3) mediates transition zone and axoneme formation of mouse photoreceptors. *J. Biol. Chem.* **290,** 12765–12778
20. Avasthi, P., Watt, C. B., Williams, D. S., Le, Y. Z., Li, S., Chen, C. K., Marc, R. E., Frederick, J. M., and Baehr, W. (2009) Trafficking of membrane proteins to cone but not rod outer segments is dependent on heterotrimeric kinesin-II. *J. Neurosci.* **29,** 14287–14298
21. Pujic, Z., and Malicki, J. (2004) Retinal pattern and the genetic basis of its formation in zebrafish. *Semin. Cell Dev. Biol.* **15,** 105–114
22. Larison, K. D., and Bremiller, R. (1990) Early onset of phenotype and cell patterning in the embryonic zebrafish retina. *Development* **109,** 567–576
23. Fadool, J. M. (2003) Development of a rod photoreceptor mosaic revealed in transgenic zebrafish. *Dev. Biol.* **258,** 277–290
24. Ile, K. E., Kassen, S., Cao, C., Vihtehlic, T., Shah, S. D., Mousley, C. J., Alb, J. G., Jr., Huijbregts, R. P., Stearns, G. W., Brockerhoff, S. E., Hyde, D. R., and Bankaitis, V. A. (2010) Zebrafish class 1 phosphatidylinositol transfer proteins: PITPβ and double cone cell outer segment integrity in retina. *Traffic* **11,** 1151–1167
25. Zhao, C., and Malicki, J. (2011) Nephrocystins and MKS proteins interact with IFT particle and facilitate transport of selected ciliary cargos. *EMBO J.* **30,** 2532–2544
26. Tam, B. M., Moritz, O. L., Hurd, L. B., and Papermaster, D. S. (2000) Identification of an outer segment targeting signal in the COOH terminus of rhodopsin using transgenic *Xenopus laevis*. *J. Cell Biol.* **151,** 1369–1380
27. Takechi, M., Hamaoka, T., and Kawamura, S. (2003) Fluorescence visualization of ultraviolet-sensitive cone photoreceptor development in living zebrafish. *FEBS Lett.* **553,** 90–94
28. Chen, Z., Song, Z., Wang, Y., and Zhao, C. (2015) Establishment of a transgenic zebrafish line with tdTomato expression in the ultraviolet-sensitive cone photoreceptors. *Acta Laboratorium Animalis Scientia Sinica* **23,** 453–457
29. Yin, J., Brocher, J., Linder, B., Hirmer, A., Sundaramurthi, H., Fischer, U., and Winkler, C. (2012) The 1D4 antibody labels outer segments of long double cone but not rod photoreceptors in zebrafish. *Invest. Ophthalmol. Vis. Sci.* **53,** 4943–4951
30. Schmitt, E. A., and Dowling, J. E. (1996) Comparison of topographical patterns of ganglion and photoreceptor cell differentiation in the retina of the zebrafish, *Danio rerio*. *J. Comp. Neurol.* **371,** 222–234
31. Lytton, J., Westlin, M., and Hanley, M. R. (1991) Thapsigargin inhibits the sarcoplasmic or endoplasmic reticulum Ca-ATPase family of calcium pumps. *J. Biol. Chem.* **266,** 17067–17071
32. Hao, L., Thein, M., Brust-Mascher, I., Civelekoglu-Scholey, G., Lu, Y., Acar, S., Prevo, B., Shaham, S., and Scholey, J. M. (2011) Intraflagellar transport delivers tubulin isotypes to sensory cilium middle and distal segments. *Nat. Cell Biol.* **13,** 790–798
33. Craft, J. M., Harris, J. A., Hyman, S., Kner, P., and Lechtreck, K. F. (2015) Tubulin transport by IFT is upregulated during ciliary growth by a cilium-autonomous mechanism. *J. Cell Biol.* **208,** 223–237
34. Young, R. W. (1967) The renewal of photoreceptor cell outer segments. *J. Cell Biol.* **33,** 61–72
35. Young, R. W. (1969) A difference between rods and cones in the renewal of outer segment protein. *Invest. Ophthalmol.* **8,** 222–231
36. Sedmak, T., and Wolfrum, U. (2011) Intraflagellar transport proteins in ciliogenesis of photoreceptor cells. *Biol. Cell* **103,** 449–466
37. Sedmak, T., and Wolfrum, U. (2010) Intraflagellar transport molecules in ciliary and nonciliary cells of the retina. *J. Cell Biol.* **189,** 171–186
38. König, B., Arendt, A., McDowell, J. H., Kahlert, M., Hargrave, P. A., and Hofmann, K. P. (1989) Three cytoplasmic loops of rhodopsin interact with transducin. *Proc. Natl. Acad. Sci. U.S.A.* **86,** 6878–6882
39. Kisselev, O. G., Downs, M. A., McDowell, J. H., and Hargrave, P. A. (2004) Conformational changes in the phosphorylated C-terminal domain of rhodopsin during rhodopsin arrestin interactions. *J. Biol. Chem.* **279,** 51203–51207
40. Kang, Y., Gao, X., Zhou, X. E., He, Y., Melcher, K., and Xu, H. E. (2016) A structural snapshot of the rhodopsin-arrestin complex. *FEBS J.* **283,** 816–821
41. Mendez, A., Burns, M. E., Roca, A., Lem, J., Wu, L. W., Simon, M. I., Baylor, D. A., and Chen, J. (2000) Rapid and reproducible deactivation of rhodopsin requires multiple phosphorylation sites. *Neuron* **28,** 153–164
42. Apfelstedt-Sylla, E., Kunisch, M., Horn, M., Rüther, K., Gerding, H., Gal, A., and Zrenner, E. (1993) Ocular findings in a family with autosomal dominant retinitis pigmentosa and a frameshift mutation altering the carboxyl terminal sequence of rhodopsin. *Br. J. Ophthalmol.* **77,** 495–501
43. Song, X., Vishnivetskiy, S. A., Gross, O. P., Emelianoff, K., Mendez, A., Chen, J., Gurevich, E. V., Burns, M. E., and Gurevich, V. V. (2009) Enhanced arrestin facilitates recovery and protects rods lacking rhodopsin phosphorylation. *Curr. Biol.* **19,** 700–705
44. Alfinito, P. D., and Townes-Anderson, E. (2002) Activation of mislocalized opsin kills rod cells: a novel mechanism for rod cell death in retinal disease. *Proc. Natl. Acad. Sci. U.S.A.* **99,** 5655–5660
45. Cideciyan, A. V., Hood, D. C., Huang, Y., Banin, E., Li, Z. Y., Stone, E. M., Milam, A. H., and Jacobson, S. G. (1998) Disease sequence from mutant rhodopsin allele to rod and cone photoreceptor degeneration in man. *Proc. Natl. Acad. Sci. U.S.A.* **95,** 7103–7108
46. Chang, N., Sun, C., Gao, L., Zhu, D., Xu, X., Zhu, X., Xiong, J. W., and Xi, J. J. (2013) Genome editing with RNA-guided Cas9 nuclease in zebrafish embryos. *Cell Res.* **23,** 465–472
47. Zhao, C., and Malicki, J. (2007) Genetic defects of pronephric cilia in zebrafish. *Mech. Dev.* **124,** 605–616
48. Leventea, E., Hazime, K., Zhao, C., and Malicki, J. (2016) Analysis of cilia structure and function in zebrafish. *Methods Cell Biol.* **133,** 179–227